



Elasticity deformation and failure modes behavior of hybrid composite CFRP/GFRP under tensile loading



Ahmad Fuad Ab Ghani ^{1,2,*}, Ghazali Omar ³, Muhammad Zaki Sulaiman ⁴, Aidah Jumahat ¹, Jamaluddin Mahmud ¹

¹Faculty of Mechanical Engineering, Universiti Teknologi MARA (UiTM), Shah Alam, Selangor, Malaysia

²Faculty of Engineering Technology (Mechanical), Universiti Teknikal Malaysia Melaka (UTeM), Taman Tasik Utama, 75450, Melaka, Malaysia

³Faculty of Mechanical Engineering, Universiti Teknikal Malaysia Melaka (UTeM), Taman Tasik Utama, 75450, Melaka, Malaysia

⁴STRATA Manufacturing PJSC, PO Box 86519, Al-Ain, UAE

ARTICLE INFO

Article history:

Received 3 October 2017

Received in revised form

9 January 2018

Accepted 13 January 2018

Keywords:

Digital image correlation

Hybrid composite

Ncorr

Non-contact strain

Failure mode hybrid composite

ABSTRACT

This article presents experimental protocol in measuring deformation occur on in-plane hybrid composites CFRP/GFRP as well as assessing the failure modes associated with them. The challenging task of extracting mechanical properties of a hybrid composite is assisted with the use of Digital Image Correlation Technique (DIC). DIC is an innovative technique which able to capture full field deformation of tensile deformation. The complex deformation captured for hybrid composite in-plane tensile deformation and behavior using Digital Image Correlation (DIC) under static loading is a new area of study in literature. Generally, hybrid composite consists of more than one reinforcing sections or multiple reinforcing or multiple matrix sections or single reinforcing phase with multiple matrix phases. As a result of the compromise between the materials within the hybrid composite, the deformation and stress analysis are to be evaluated and tailored as each constituent of material carry their own desired mechanical properties according to a performance requirement. It is found from a classical relation of stress-strain relationship of the hybrid composite under tensile loading, the modulus of elasticity is found to record value around 100839 MPa and 80778 MPa which in theoretical benchmark located in between value of Modulus of Elasticity for CFRP (120 GPa) and GFRP (36 GPa) which proves the occurrence of hybrid effect.

© 2018 The Authors. Published by IASE. This is an open access article under the CC BY-NC-ND license (<http://creativecommons.org/licenses/by-nc-nd/4.0/>).

1. Introduction

The major challenge for the composite engineer is to develop of new stronger, tough and lightweight materials to supporting the latest design concept for complex shape structural. Composite are attractive material because of their properties such as high strength and stiffness leads to the application in the area marine, aerospace and automotive. A composite material also can be defined as a combination of a matrix and reinforcement (Nettles, 1994). Tensile test is one of the mechanical testings that evaluating fundamental properties of engineering materials as well as in developing new materials and in controlling the quality of materials for use in design and construction.

The main parameter that can obtain during the tensile test is Ultimate Tensile Strength (UTS), Yield Strength (σ_y), Elastic Modulus (E), Poisson Ratio (ν), and percent elongation percent elongation (ΔL) (Miracle and Donaldson, 2001). The standard method for tensile testing polymer matrix composites was described by ASTM D3039. Generally, hybrid composite consists of more than one reinforcing sections or multiple reinforcing or multiple matrix sections or single reinforcing phase with multiple matrix phases. As a result of a compromise between the materials within the hybrid composite, the deformation and stress analysis are to be evaluated and tailored as each constituent of material carry their own desired mechanical properties according to the performance requirement. A digital camera is used to capture the consecutive image during deformation and change the surface characteristics while load increase. This technique starts with the reference image as a static image and when the load applied the picture will snap during deformation occur as a deformed image.

* Corresponding Author.

Email Address: ahmadfuad@utem.edu.my (A. F. A. Ghani)

<https://doi.org/10.21833/ijaas.2018.03.014>

2313-626X/© 2018 The Authors. Published by IASE.

This is an open access article under the CC BY-NC-ND license

(<http://creativecommons.org/licenses/by-nc-nd/4.0/>)

2. Digital image correlation technique

Digital Image Correlation is a non-contact, optical method which captures of digital images of a surface of an object then performs the image analysis to obtain full-field deformation and measurements. This can be achieved by creating different methods like dots, grids, lines etc., on the specimen surface (Huang and Zhang, 2010). This technique starts with a reference image (before loading) followed by a series of pictures taken during the deformation. Deformed images show a different dot pattern relative to the initial non deformed reference image. These patterns difference can be calculated by performing correlation of the pixels of the reference image and any deformed image and a full-field displacement measurement can be computed. The strain distribution can then be obtained by applying the derivatives in the displacement field (Skozrit et al., 2015). To apply this method, the object under study needs to be prepared with random dot pattern speckle pattern to its surface.

For surface deformation computation utilizing 2D Digital Image Correlation (DIC) technique, emphasized should be given on positioning of specimen under testing, light intensity and sources as well as camera lens and its capability/resolution/frame rate of camera. Accurate measurement relies heavily on imaging system configuration. In principle, sample with random speckle pattern sprayed on the surface must be positioned perpendicular to the camera to avoid any out of plane motion. After the entire load applied events, a series of images are taken before and after loading and deformation and finally stored in the computer for post processing images to obtain displacement contour/field using DIC algorithm. Basically from technical perspectives, for 2D DIC, image resolution plays a vital role in measurement accuracy (Blaber et al., 2015). Fig. 1 shows the fundamental principle of digital image correlation.

3. Methodology

High speed camera used for DIC for this research contains the sensor recording speeds of up to 200,000fps and 800 x 600 resolutions at 1000fps, Camera Display Unit (CDU) built in measurement, and storage and editing capability. Olympus I-Speed 2 camera is used to capture images for tensile and bending test. The features contain the sensor recording speeds of up to 200,000fps and 800 x 600 resolutions at 1000fps, Camera Display Unit (CDU) built in measurement and storage and editing capability. Olympus I-Speed 2 camera is used to capture images for tensile and bending test. DIC system use optic method through stereoscopic sensor arrangement to analyze the deformation of object and emphasis on each point subset based on grey value of digital image to define the strain (Wei et al., 2013). The camera is positioned perpendicular to the specimen under testing (Fig. 2). In order for the digital image correlation algorithm able to

perform the correlation analysis, speckle pattern must be sprayed onto the surface of the coupon (Fig. 3). The pattern must be contrast enough and small enough to capture the deformation. The technical specification of the high speed camera is a high speed camera with frequency 60 – 200,000 frame per second, shutter minimum of 1 microsecond, a Nikkor 18-55 mm lense, open source software for DIC which is Ncorr platform, with installed Matlab version of 2012 and Microsoft Visual C++ as compiler.

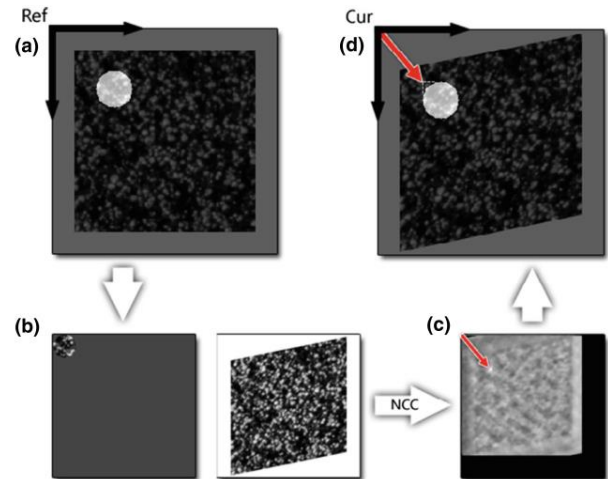


Fig. 1: (a) A reference subset (b) Expanded to full size (c) Superimposed with the current image for correlation (d) Subset recovered via positioning the maximum correlation coefficient (Blaber et al., 2015)

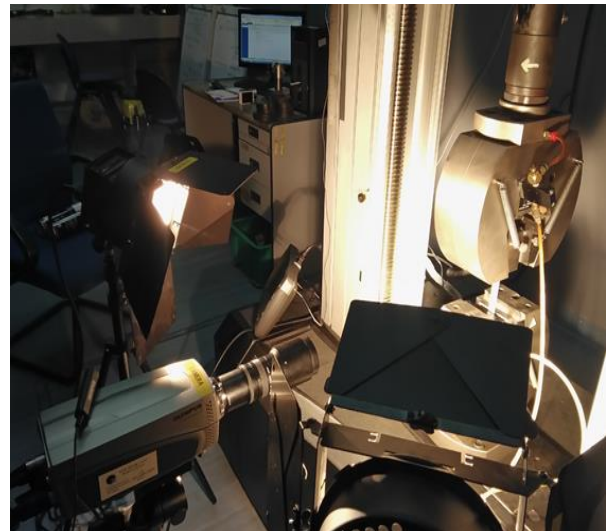


Fig. 2: Setting up of DIC on tensile test specimen under study (CFRP, GFRP and hybrid composite CFRP/GFRP)

3.1. Sample preparation

The prepreg is layup as per desired design requirement (sequence of layup and finer orientation). Metal plate is cleaned using wax to remove any dirt. The pressure is set to 6 bar which includes 5 bar set in the machine hot press and 1bar from vacuum bag. Temperature is set to 120°C and let the temperature to be stable. Composite layups (prepreg layup) inside the vacuum bag is placed between the metal plates and the proses of hot press

as per intended pressure will take place. The dimension of the specimen has to follow the standard used, which is ASTM D3039. Fig. 3a depicts the speckle pattern sprayed onto the tensile test coupon of hybrid composite under study as well as its layup arrangement which comprises of CFRP and GFRP layers hybrid composite (2 types) as shown in Fig. 3b.



Fig. 3a: Hybrid Composite CFRP/GFRP cut as per ASTM D3039 with speckle sprayed onto surface

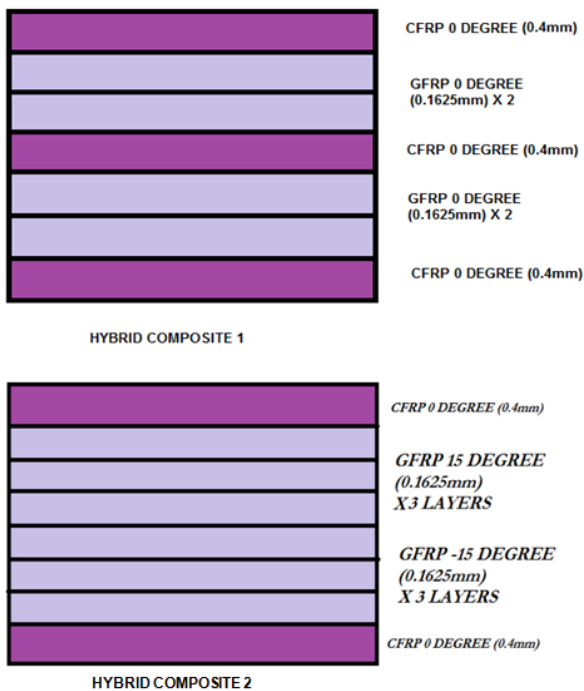


Fig. 3b: Two different configurations of hybrid composite CFRP/GFRP under study

3.2. Formatting displacements

The Ncorr opensource platform requires user to input and define its displacement format which include the measurement calibration and scale. These options were used to convert the displacements from pixels to real units. The real value of width of the specimen directly inserts at the “# of Units” for example 20 mm as shown in Fig. 4.

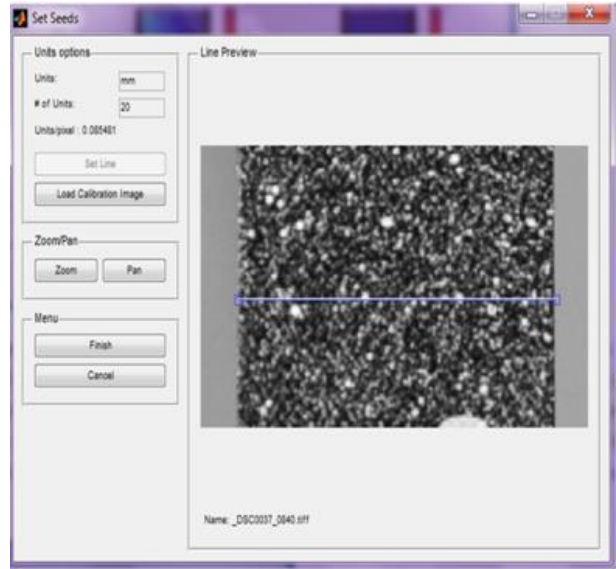


Fig. 4: Scaling the pixels captured via high speed camera into in plane length measurement in mm

3.3. Calculation of strains using Ncorr

The selection of the ideal strain radius is similar to the selection of the ideal subset radius, in that the smallest radius was desired which does not result in noisy strain data. The radius normally set to 13 because of the optimal radius as shown in Fig. 5. Lastly, it was assumed either the displacement has been formatted or the strain has been calculated. This was the last step of the analysis. The value of the strain shown in the direction of ϵ_{xx} , ϵ_{xy} and ϵ_{yy} as below, Fig. 6, Fig. 7 and Fig. 8 respectively.

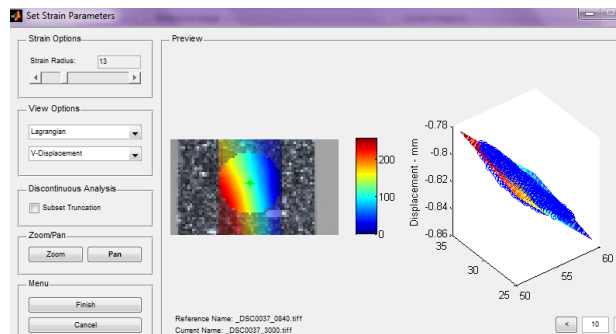


Fig. 5: Computation of strain with selection of radius covered in Ncorr open source platform

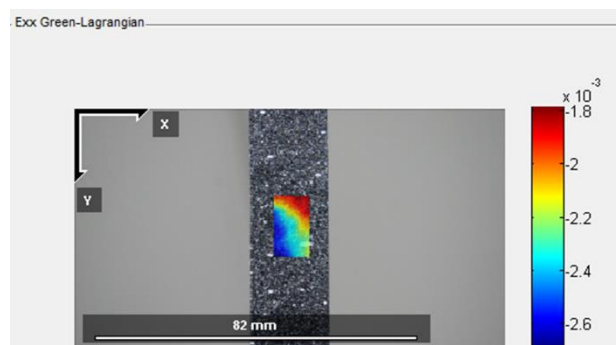


Fig. 6: Strain contour in transverse direction (Equivalent to xx in global axis) obtained using Ncorr

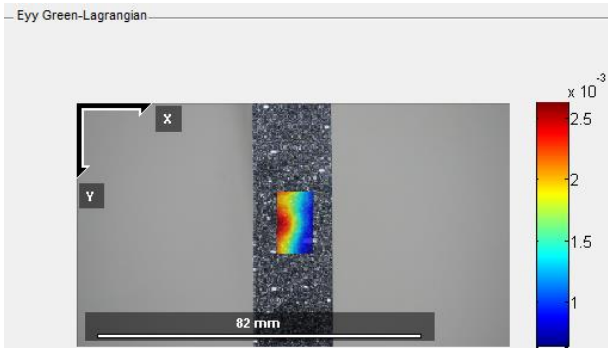


Fig. 7: Strain contour in longitudinal direction (Equivalent to ϵ_{yy} in global axis) obtained using Ncorr

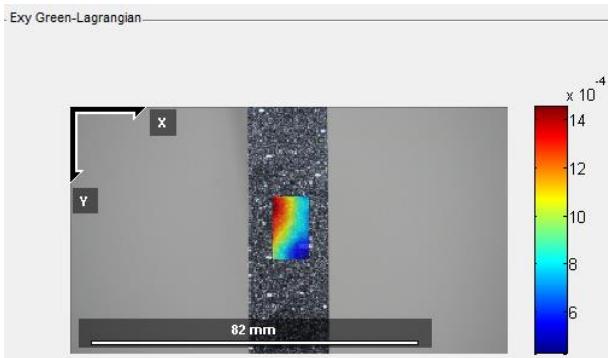


Fig. 8: Strain contour in shear direction (Equivalent to ϵ_{xy} in global axis) obtained using Ncorr

3.4. Mechanics of composite

In understanding the deformation which translated in the form of stress strain relationship and strain computation using digital image correlation (DIC) via Ncorr postprocessing software, it is very essential to relate with fundamental mechanics of composite. The mechanics of composite stress strain formulation which based on Composite Laminate Theory (CLT) is very useful in comprehending the effect of different layup and orientation of plies on computation of strain value in xx , yy and xy (shear strain) which then affecting the computation of effective modulus of elasticity, E_{11} (longitudinal direction). In regards of hybrid composite CFRP/GFRP under study, it is aimed to visualize and compute from DIC method, shear strain, ϵ_{xy} contour and profile for hybrid composite at on inplane surface. This is explained further in Section 5.0 (Discussion) later. The stress strain relationship is an essential principle for mechanics of composite study. Material under study; CFRP and GFRP are both unidirectional composites which possess orthotropic material properties which has different elasticity deformation behavior at longitudinal and transversal direction with respect to fiber orientation. For an orthotropic system, the stress strain relationship is given as follows:

$$\sigma_1 = E_1 \epsilon_1 \text{ and } \sigma_2 = E_2 \epsilon_1 \quad (1)$$

where E_1 and E_2 are the two elastic constants. Poisson's ratio is defined as the strain perpendicular to a given load direction to the strain parallel to a given load direction (Nettles, 1994).

$$\nu_{12} = \frac{\epsilon_T}{\epsilon_L} = \frac{\epsilon_2}{\epsilon_1} \quad (2)$$

Thus, stress and strain components in terms of Poisson's ratio are given as follows:

$$\begin{aligned} \epsilon_1 &= \frac{\sigma_1}{E_1} - \nu_{21} \epsilon_2 \\ \epsilon_2 &= \frac{\sigma_2}{E_2} - \nu_{12} \epsilon_1 \end{aligned} \quad (3)$$

The relationship between shear stress, strain and bulk Modulus is given as follows:

$$\tau_{12} = \gamma_{12} G_{12} \quad (4)$$

Using the above relations, the relation between the stress and strain in terms of the compliance matrix and the stiffness matrix are given as follows (Nettles, 1994; Okutan, 2001):

$$\begin{bmatrix} \epsilon_1 \\ \epsilon_2 \\ \gamma_{12} \end{bmatrix} = \begin{bmatrix} S_{11} & S_{12} & 0 \\ S_{12} & S_{22} & 0 \\ 0 & 0 & S_{66} \end{bmatrix} \begin{bmatrix} \sigma_1 \\ \sigma_2 \\ \tau_{12} \end{bmatrix} \quad (5)$$

$$\begin{bmatrix} \sigma_1 \\ \sigma_2 \\ \tau_{12} \end{bmatrix} = \begin{bmatrix} Q_{11} & Q_{12} & 0 \\ Q_{12} & Q_{22} & 0 \\ 0 & 0 & Q_{66} \end{bmatrix} \begin{bmatrix} \epsilon_1 \\ \epsilon_2 \\ \gamma_{12} \end{bmatrix} \quad (6)$$

where $[S]$ matrix is the compliance matrix and $[Q]$ is the stiffness matrix. Here

$$Q_{11} = \frac{E_1}{1 - \nu_{12}\nu_{21}}, \quad Q_{22} = \frac{E_2}{1 - \nu_{12}\nu_{21}} \text{ and } Q_{12} = Q_{21} = \frac{\nu_{21}E_1}{1 - \nu_{12}\nu_{21}} \quad (7)$$

If the lamina is loaded at some angle other than 0 degree or 90 degree The stresses and strains will not be the same since they are vectors and therefore a relation needs to be derived which considers the general angle at which the lamina are oriented. Therefore the generalized equation in matrix form relating the principal stresses with directional stresses is given as follows: (Nettles, 1994; Miracle and Donaldson, 2001; Okutan, 2001).

$$\begin{bmatrix} \sigma_1 \\ \sigma_2 \\ \sigma_3 \end{bmatrix} = [T] \begin{bmatrix} \sigma_x \\ \sigma_y \\ \tau_{xy} \end{bmatrix} \quad (7)$$

where $[T]$ which is called the transformation matrix is given as follows:

$$[T] = \begin{bmatrix} \cos^2 \theta & \sin^2 \theta & 2 \sin \theta \cos \theta \\ \sin^2 \theta & \cos^2 \theta & -2 \sin \theta \cos \theta \\ -\sin \theta \cos \theta & \sin \theta \cos \theta & \cos^2 \theta - \sin^2 \theta \end{bmatrix} \quad (8)$$

similarly for strain,

$$\begin{bmatrix} \epsilon_1 \\ \epsilon_2 \\ \epsilon_3 \end{bmatrix} = [T] \begin{bmatrix} \epsilon_x \\ \epsilon_y \\ \epsilon_{xy} \end{bmatrix} \quad (9)$$

Expressing the directional stresses and strains in terms of lamina stiffness matrix, it is given as:

$$\begin{bmatrix} \sigma_x \\ \sigma_y \\ \tau_{xy} \end{bmatrix} = \begin{bmatrix} \overline{Q}_{11} & \overline{Q}_{12} & 2\overline{Q}_{16} \\ \overline{Q}_{12} & \overline{Q}_{22} & 2\overline{Q}_{26} \\ \overline{Q}_{16} & \overline{Q}_{26} & 2\overline{Q}_{66} \end{bmatrix} \begin{bmatrix} \epsilon_x \\ \epsilon_y \\ \epsilon_{xy} \end{bmatrix} \quad (11)$$

3.5. Constitutive equations for strains and stresses

The constitutive equations that relate stress and strain behavior of composite laminate based on Composite Laminate Theory which gives understanding on behavior with respect to extension, bending and coupling of composite laminate.

The stress and the moment resultants relation are given by:

$$\begin{aligned}
 N_x &= \int_{-\frac{h}{2}}^{\frac{h}{2}} \sigma_x dz & M_x &= \int_{-\frac{h}{2}}^{\frac{h}{2}} \sigma_x z dz \\
 N_y &= \int_{-\frac{h}{2}}^{\frac{h}{2}} \sigma_y dz & M_y &= \int_{-\frac{h}{2}}^{\frac{h}{2}} \sigma_y z dz \\
 N_{xy} &= \int_{-\frac{h}{2}}^{\frac{h}{2}} \tau_{xy} dz & M_{xy} &= \int_{-\frac{h}{2}}^{\frac{h}{2}} \tau_{xy} z dz
 \end{aligned} \tag{12}$$

Writing the Eq. 14 in the matrix form and generalizing the equation for stress and moment resultants in terms of the mid plane strains and the curvature corrections, the equations are written as follows:

$$\begin{bmatrix} N_x \\ N_y \\ N_{xy} \end{bmatrix} = \sum_{k=1}^n \{ [\bar{Q}]_k \begin{bmatrix} \varepsilon_x^0 \\ \varepsilon_y^0 \\ \gamma_{xy}^0 \end{bmatrix} \int_{h_{k-1}}^{h_k} dz + [\bar{Q}]_k \begin{bmatrix} K_x \\ K_y \\ K_{xy} \end{bmatrix} \int_{h_{k-1}}^{h_k} z dz \} \tag{13}$$

Combining the laminate terms and the h terms to define A, B, D matrices which can be written as (Nettles, 1994):

$$\begin{aligned}
 A_{ij} &= \sum_{k=1}^n [\bar{Q}_{ij}]_k (h_k - h_{k-1}) \\
 B_{ij} &= \sum_{k=1}^n [\bar{Q}_{ij}]_k (h_k^2 - h_{k-1}^2) \\
 D_{ij} &= \sum_{k=1}^n [Q_{ij}]_k (h_k^3 - h_{k-1}^3).
 \end{aligned} \tag{15}$$

In matrix form, the constitutive equations are given as follows:

$$\begin{bmatrix} N_x \\ N_y \\ N_{xy} \\ M_x \\ M_y \\ M_{xy} \end{bmatrix} = \begin{bmatrix} A_{11} & A_{12} & A_{16} & B_{11} & B_{12} & B_{16} \\ A_{12} & A_{22} & A_{26} & B_{12} & B_{22} & B_{26} \\ A_{16} & A_{26} & A_{66} & B_{16} & B_{26} & B_{66} \\ B_{11} & B_{12} & B_{16} & D_{11} & D_{12} & D_{16} \\ B_{12} & B_{22} & B_{26} & D_{12} & D_{22} & D_{26} \\ B_{16} & B_{26} & B_{66} & D_{16} & D_{26} & D_{66} \end{bmatrix} \begin{bmatrix} \varepsilon_x^0 \\ \varepsilon_y^0 \\ \gamma_{xy}^0 \\ K_x \\ K_y \\ K_{xy} \end{bmatrix} \tag{16}$$

The cross sectional forces and moments can be determined by the summation of the integrated stress components over each individual ply. The result is the so called ABD matrix, which relates the cross-sectional forces and moments to mid plane strains and curvatures.

4. Results

4.1. Output from Ncorr postprocessing

The output from Ncorr platform are obtained in the form of quantification of contour displacement in X and Y direction (global axis) which represented in

the notation of U and V as in Ncorr platform. The other essential readings and findings are strain in xx, strain in yy (loading direction/tensile direction) and in plane shear strain, xy direction. Fig. 9 depicts the displacement in Y for Hybrid composite 1 at 2000 N and Fig. 10 correspond to load at 7 KN.



Fig. 9: Contour of displacement in longitudinal direction (Equivalent to yy in global axis) for hybrid 1 at 2000 N tensile load

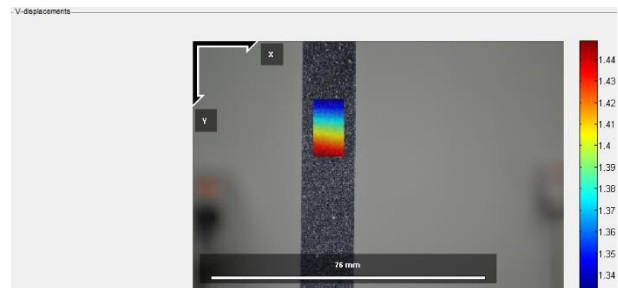


Fig. 10: Contour of displacement in longitudinal direction (Equivalent to yy in global axis) for hybrid 1 at 7000 N tensile load

Fig. 11 shows the strain in yy direction (tensile loading direction) for hybrid composite correspond to 4000 N while Fig. 12 depicts increment of strain yy at 7000 N.

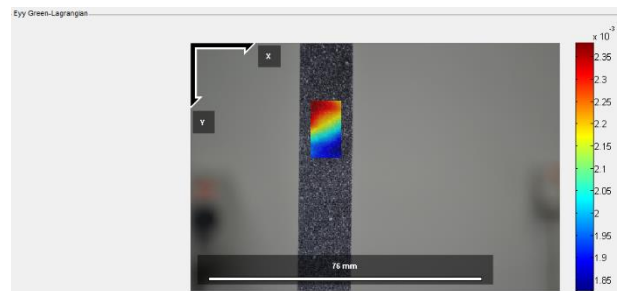


Fig. 11: Contour of strain in longitudinal direction (Equivalent to yy in global axis) for hybrid 1 at 7000 N tensile load

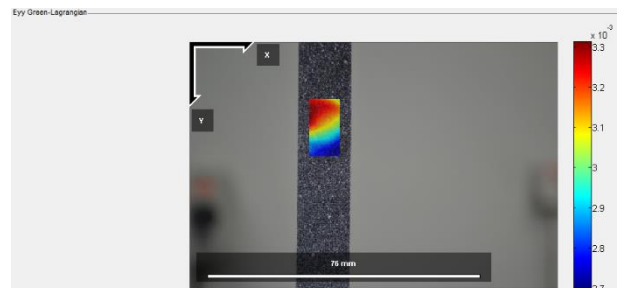


Fig. 12: Contour of strain in longitudinal direction (Equivalent to yy in global axis) for hybrid 1 at 4000 N tensile load

Fig. 13 shows the contour plot of strain in transverse direction that corresponds to 7000 N. Contraction expected to occur for tensile loading coupon, which shows the poisson effect for the CFRP and GFRP layers forming the hybrid laminate. Fig. 14 show the in plane shear strain xy, full field contour at 3500 N where it accounts mostly near zero proximity due to the fact that it is unidirectional 0 degree with respect to tensile loading for both CFRP and GFRP respectively. Meanwhile for Fig. 15, which represents higher tensile loading acting on the specimen, the in plane shear is higher in terms of value, 0.0011 which hypothesisly might due to the poisson effect, compatibility phenomena between plies of CFRP/GFRP that has different modulus of elasticity.

Fig. 16 depicts the graph of stress (longitudinal direction) against strain (longitudinal direction) for CFRP, GFRP and Hybrid Composite 1 and Hybrid Composite 2. It is seen that Hybrid 1 plot gradient which represents the Modulus of Elasticity, E in longitudinal direction is quite close with the one computed from CFRP 0 Degree.

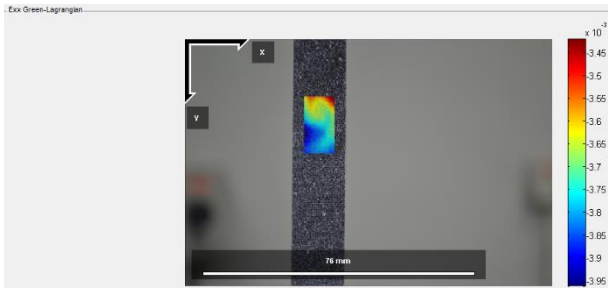


Fig. 13: Contour strain in transverse direction (XX in global axis) for hybrid #1 composite at 7000 N

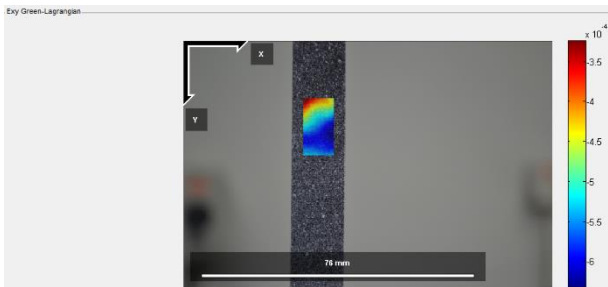


Fig. 14: Contour strain in shear direction (XY in global axis) for hybrid #1 composite at 3500 N

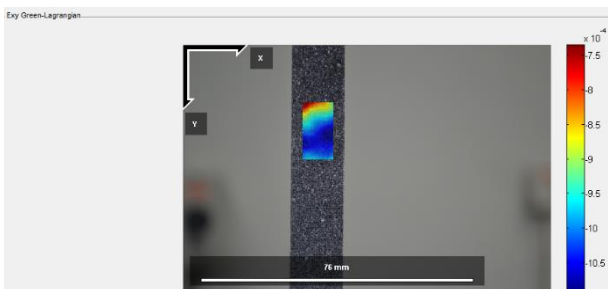


Fig. 15: Contour of displacement in shear direction (Equivalent to xy in global axis) for hybrid 1 at 6500 N tensile load

Fig. 17a shows the relationship of Stress (Longitudinal Direction) which equivalent to σ_{yy} in

Global Axis against Strain (Longitudinal Direction) for Hybrid Composite #1. The Tensile Strength, TS recorded at 709.69 MPa as delamination failure mode is observed.

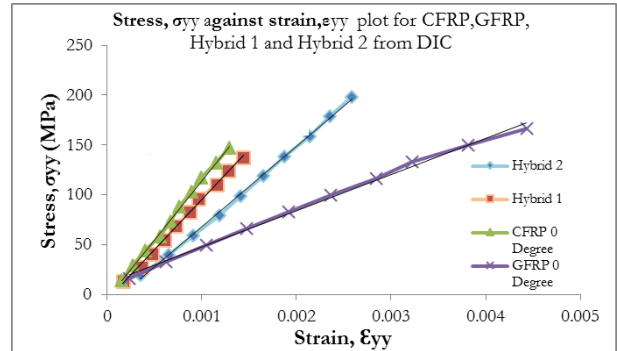


Fig. 16: Graph of stress (longitudinal direction) against strain (longitudinal direction) for CFRP, GFRP and hybrid composite

Fig. 17b depicts the relation of Stress (Longitudinal Direction) which equivalent to σ_{yy} in Global Axis against Strain (Longitudinal Direction) for Hybrid Composite #2. The Tensile Strength, TS recorded at 587 MPa as shear dominated failure of GFRP and delamination at the interface of CFRP/GFRP were seen as major factors reducing the Tensile Strength of Hybrid Composite #2.

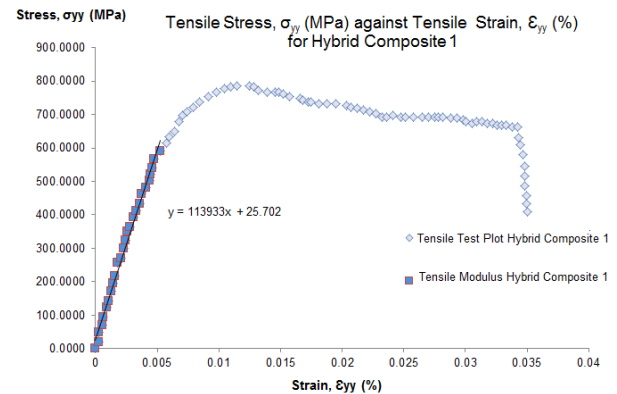


Fig. 17a: Graph of stress (longitudinal direction) against strain (longitudinal direction) for hybrid composite #1

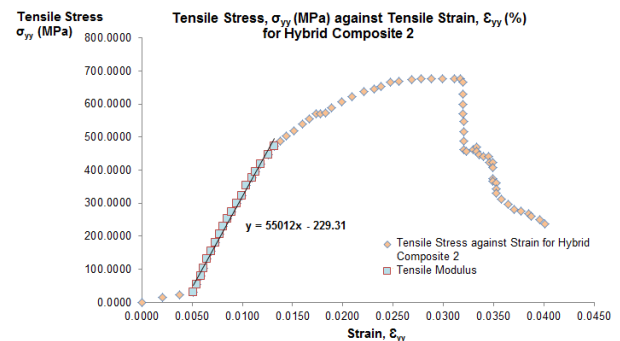


Fig 17b: Graph of Stress (longitudinal direction) against strain (longitudinal direction) for hybrid composite #1

Table 1 summarizes the modulus of elasticity, E_{11} in the longitudinal direction (tensile loading direction) and Tensile Strength for CFRP, GFRP, Hybrid Composite #1 and Hybrid Composite #2 obtained from experiment.

Table 1: Modulus of elasticity, E_{11} (MPa) and tensile strength, UTS (MPa) for all the composite

	E_{11} (MPa)	Tensile Strength(MPa)
CFRP 0 Degree	118430	1261
GFRP 0 Degree	36288	866
Hybrid 1	100839	709.69
Hybrid 2	80778	583.89

4.2. Failure mode of hybrid composite CFRP/GFRP

Fig. 18 shows the condition of sample Hybrid 2 after undergo tensile test. Sample Hybrid 2 is a sandwich between Two (2) external layers of CFRP with 15 degree angle fiber orientation of GFRP which account for five (5) layers. The microstructure view shows clearly the failure mode occurs is matrix cracking at the shear principal direction of 15 and delamination between CFRP/GFRP. Fig. 18 and Fig. 19 depict the catastrophic rupture occur on GFRP lamina. Glass fibers were separated from matrix fiber bridging occurs that also brought into delamination, matrix cracking and propagation. On the other hand, the phenomenon of fiber bridging in the CFRP lamina is quite minimal with little amount of fiber seen separated.

Fig. 19 shows the sequence of failure of sample Hybrid 2 from initiation, propagation and total failure. Shear failure in GFRP region with delamination taking place at area 2. At area 1, cracking of matrix initiate, propagate and travelled cross section in CFRP. Outer layer of CFRP region 3 is continuation of delamination effect taking place from GFRP layer (15° fiber direction) where interlayer cracking occurs.

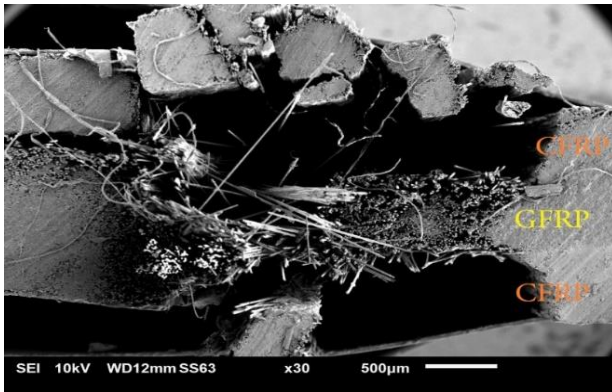


Fig. 18: Microstructure view of sample Hybrid 2

Composite Hybrid 1 consists of 7 layers which are CFRP-2XGFRP-CFRP-2XGFRP-CFRP. Fig. 20 and Fig. 21 shows the SEM view of failed sample of Hybrid Composite 1. Fig. 20 shows matrix cracking initiates at point 1 enter CFRP and GFRP region until point 2. At point 2, CFRP fibers were seen separated from each other also known as fiber bridging phenomenon that brought to final fracture. Fig. 21 shows different sample of failed Composite Hybrid 1. There are two (2) significant failures behaviour observed; interlayer delamination started and followed by stress concentration which induced to matrix crackin. Carbon fibers and matrix tend to be

strong bonding since less fiber separated/bridging observed as compared to glass fiber.

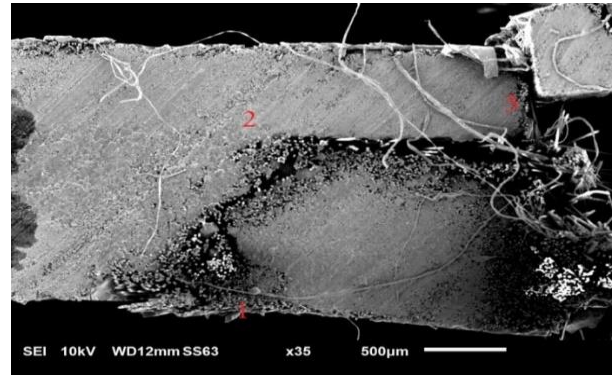


Fig. 19: Cross section view of failed sample Hybrid 2

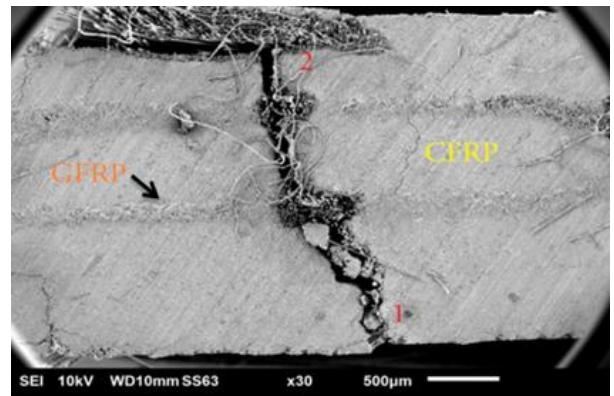


Fig. 20: Microstructure view of ruptured sample 1 (up to failure) for Hybrid 1

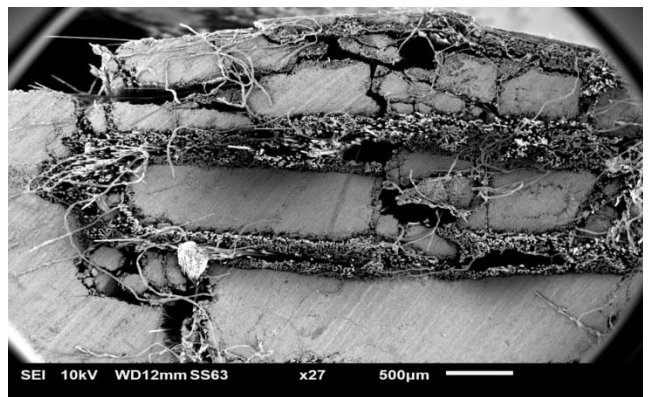


Fig. 21: Microstructure view of ruptured sample 2 (up to failure) for Hybrid 1

5. Discussion

Approximation of Modulus of Elasticity, E in yy direction for hybrid composite is calculated using Eq. 1, where strain of yy is obtained from DIC method described before. Stress in yy direction which acted on the principal direction of hybrid composite, is computed with the relation of force divided by cross section area of hybrid composite tensile coupon under loading. Digital Image Correlation technique is able to provide full field measurement that includes the transverse strain, ϵ_{xx} and in plane shear strain, ϵ_{xy} . It is observed from contour of shear strain, ϵ_{xy} in Fig. 14 and Fig. 15 that there is substantial increment of shear strain magnitude recorded with increment

of load and this phenomenon could be explained in the coupling terms involved as well poisson effect with different modulus of elasticity, E_{11} between CFRP and GFRP composite material forming the Hybrid 1 composition. The modulus of elasticity in longitudinal direction for CFRP is around 120 GPa and modulus of elasticity for GFRP unidirectional 0 degree as accordance to ASTM D3039 is in the range of 35 to 40 GPa. Hence the value obtained from DIC for hybrid composite, is expected to locate within the proximity range in between CFRP and GFRP. The figure computed from Eq. 1 approaches 100.8 GPa is explained with the fact that CFRP layers (3 layers as per layup) play dominant factor in stress strain behavior of hybrid composite where CFRP acts as load bearer relatively higher than counterpart constituent GFRP as compared to Hybrid 2 which recorded lower Modulus of Elasticity, E_{11} [80.78 GPa] due to the presence of 15° fiber orientation of GFRP in between two layers of CFRP which induced significant contribution towards shearing effect on principal direction of GFRP. This could be explained fundamentally from the stress transformation at principal direction that can be extracted from Eq. 8 and Eq. 9. The failure mode which seen from Hybrid Composite 2 is mainly predominant by shear effect from GFRP. It is justified with analytical formulation using classical lamination theory embedding Hybrid Composite 2 CFRP/GFRP laminates where coupling between extensional and shear as well as extensional and twisting elements exists in the formulation as shown below originated from Eq. 13, Eq. 16 and Eq. 18:

$$A_{ij} = \sum_{k=1}^n [\bar{Q}_{ij}]_k (h_k - h_{k-1})$$

$$= \begin{bmatrix} 124.5 & 7.303 & 4.524 \\ 7.303 & 20.06 & 0.107 \\ 4.524 & 0.1070 & 8.131 \end{bmatrix} \text{ GPa-mm}$$

Meanwhile, the scenario will be very much different with benchmarking formulation if the layup of CFRP and GFRP are all parallel (all in 0° fiber direction) and computed as below:

$$A_{ij} = \begin{bmatrix} 127 & 5.954 & 0 \\ 5.954 & 19.85 & 0 \\ 0 & 0 & 6.856 \end{bmatrix} \text{ GPa-mm}$$

The coupling between extensional and shear has induced to much lower tensile strength as experienced by Hybrid Composite 2 as shown in Fig. 17 stress strain plot up to failure.

Failure modes of Hybrid Composites 1 and Hybrid Composite 2 are also assessed. Hybrid 2 which comprises of arrangement that has 5 layers of experienced the failure initiation at the region of principal direction of 15° of GFRP layers. Besides that CFRP external layers itself experiencing matrix cracking both in horizontal and vertical position as the consequence of shear failure at the principal direction of GFRP, stress concentration, crack propagation into region of CFRP. Obvious different is observed in the failure behaviour between CFRP and GFRP lamina where fiber bonding/interface where

CFRP region seems higher than GFRP where substantial amount of fiber bridging occurs. This could be explained due to the fact that shear failure play dominant role in failure initiation and failure effect. This failure phenomenon is similar in finding obtained by Shokrieh and Omid (2009) where they claimed that delamination and shear deformation were observed for off axis glass fiber during their tensile testing. In another researcher work by Ikbali et al. (2016), similar circumstance occurs and seen from failure mode perspective, where delamination, not severe, observed in the specimens and the interface between layers produced a bit more delamination. The dominant failure at compression side was expected due to occurrence of micro-buckling, shear and splitting.

As for Hybrid Composite 1, which experience significant effect of delamination between CFRP/GFRP layers than brought to other failure propagation such as combination of matrix cracking, fiber bridging and intralayer crack propagation within CFRP and GFRP laminates. This mode of failure in hybrid CFRP/GFRP is in agreement with findings from Ikbali et al. (2017) where low elongation carbon fiber is surrounded by high elongation glass fiber and this induced significantly in the delamination occurrence between CFRP/GFRP inter layer. They also observed that there was stress drop noticed in stress strain curves where load continued to increase while the stress also increased up to failure. This occurred due to the fact that the remaining of the stress was carried by glass fiber and this has also brought into little nonlinearity shown in stress strain. This is also quite similar in pattern as in Fig. 17. Meanwhile in another comprehensive research by Alessa (2014) in the study of delamination in hybrid carbon/glass fiber composites, she found that due to failure mode of fiber bridging, the cracks would alternate between the carbon and glass interfaces. The occurrence also justified with findings from SEM fractography. She also observed from the failure phenomenon that in hybrid mixed mode specimens, the cracks would go to the carbon fiber side predominantly. This failure pattern is in agreement with the one seen from SEM as per in Fig. 21.

6. Conclusion

The hybrid effect is obtained with the calculation of the modulus of elasticity for CFRP/GFRP Hybrid 1 and Hybrid 2 resulted in 100.8 GPa and 80.78 GPa respectively. This is in between the value of CFRP and GFRP alone which accounts for 120 GPa and 36 GPa respectively. Digital Image Correlation (DIC) is capable of measuring the deformation of a hybrid composite which also accounts the effect of shear strain, ϵ_{xy} on the in-plane surface of the tensile coupon. The result shows that the value of Young Modulus (E) for the hybrid composite lies between the values for the single constituent composite, CFRP and GFRP. It shows that the hybrid composite has a more favorable balance between the inherent

advantages and disadvantages of the single composite. The prime important to design the hybrid composite is a selection of the type of compatible fibers and also the level of their properties. The effect of shear from the GFRP declined the value of modulus of elasticity, E_{11} significantly for Hybrid 2. The failure mode for both Hybrid 1 and Hybrid 2 composite have been assessed where delamination between carbon fiber/glass fiber layers is significant effect inducing to other failure/rupture which includes matrix cracking, fiber bridging, and matrix fretting. Digital Image Correlation (DIC) is an innovative method measuring the deformation and value of strain. DIC is also low-cost non-contact strain measurement technique challenging the conventional method such as strain gauge, extensometer etc.

Acknowledgement

Authors would like to thank Faculty of Mechanical Engineering, Universiti Teknikal Malaysia Melaka (UTeM) for experimental facilities and and Universiti Technology MARA (UiTM), Shah Alam for technical expertise and guidance on experimental mechanics and fundamental composite engineering.

References

Blaber J, Adair B, and Antoniou A (2015). Ncorr: Open-source 2D digital image correlation Matlab software. *Experimental Mechanics*, 55(6): 1105–1122.

Huang HW and Zhang Y (2010). Dynamic application of digital image and colour processing in characterizing flame radiation

features. *Measurement Science and Technology*, 21(8): 085202. <https://doi.org/10.1088/0957-0233/21/8/085202>

Ikkal H, Wang Q, Azzam A, and Li W (2016). Effect of hybrid ratio and laminate geometry on compressive properties of carbon/glass hybrid composites. *Fibers and Polymers*, 17(1): 117-129.

Ikkal MH, Ahmed A, Qingtao W, Shuai Z, and Wei L (2017). Hybrid composites made of unidirectional T600S carbon and E-glass fabrics under quasi-static loading. *Journal of Industrial Textiles*, 46(7): 1511-1535.

Ilessa HA (2014). Delamination in hybrid carbon/glass fiber composites. Ph.D. Dissertation, University of Dayton, Dayton, USA.

Miracle DB and Donaldson SL (2001). Macromechanics analysis of laminate properties. In Miracle DB and Donaldson SL (Eds.), *ASM Handbook volume 21: Composites*: 207–211. ASM International, Geauga County, USA.

Nettles AT (1994). Basic mechanics of laminated composite plates. Technical report No. N-95-15763; NASA-RP--1351; M--764; NAS--1.61: 1351, National Aeronautics and Space Administration (NASA), Huntsville, Alabama, USA.

Okutan B (2001). Stress and failure analysis of laminated composite pinned joints. Ph.D. Dissertation, Dokuz Eylül University, İzmir, Turkey.

Shokrieh MM and Omidi MJ (2009). Tension behavior of unidirectional glass/epoxy composites under different strain rates. *Composite Structures*, 88(4): 595-601.

Skozrit I, Francfesi J, Tonkovic Z, Surjak M, Krstulovic-Opara L, Vesenjck M, Loncaric D (2015). Validation of numerical model by means of digital image correlation and thermography. *Procedia Engineering*, 101: 450–458. <https://doi.org/10.1016/j.proeng.2015.02.054>

Wei KS, Karuppanan S, and Latif MRBA (2013). Development of an optical strain measurement method using digital image correlation. *Asian Journal of Scientific Research*, 6(3): 411–422.